



1 **Ensemble streamflow forecasting over a cascade reservoir catchment with**
2 **integrated hydrometeorological modeling and machine learning**

3

4 Junjiang Liu¹, Xing Yuan^{1*}, Junhan Zeng¹, Yang Jiao¹, Yong Li², Lihua Zhong², Ling

5

Yao³

6

7 ¹School of Hydrology and Water Resources, Nanjing University of Information

8

Science and Technology, Nanjing 210044, China

9

²Guangxi Meteorological Disaster Prevention Center, Nanning 530022, China

10

³Guangxi Guiguan Electric Power Co., Ltd., Nanning 530029, China

11

12

13

14

15

16

**Corresponding author address:* Xing Yuan, School of Hydrology and Water Resources, Nanjing University of Information Science and Technology, Nanjing 210044, China E-mail: xyuan@nuist.edu.cn



17 **Abstract.** A popular way to forecast streamflow is to use bias-corrected
18 meteorological forecast to drive a calibrated hydrological model, but these
19 hydrometeorological approaches have deficiency over small catchments due to
20 uncertainty in meteorological forecasts and errors from hydrological models,
21 especially over catchments that are regulated by dams and reservoirs. For a cascade
22 reservoir catchment, the discharge of the upstream reservoir contributes to an
23 important part of the streamflow over the downstream areas, which makes it
24 tremendously hard to explore the added value of meteorological forecasts. Here, we
25 integrate the meteorological forecast, land surface hydrological model simulation and
26 machine learning to forecast hourly streamflow over the Yantan catchment, where the
27 streamflow is influenced both by the upstream reservoir water release and the
28 rainfall-runoff processes within the catchment. Evaluation of the hourly streamflow
29 hindcasts during the rainy seasons of 2013-2017 shows that the hydrometeorological
30 ensemble forecast approach reduces probabilistic forecast error by 10% and
31 deterministic forecast error by 6% as compared with the traditional ensemble
32 streamflow prediction (ESP) approach during the first 7 days. The deterministic
33 forecast error can be further reduced by 6% in the first 72 hours when combining the
34 hydrometeorological forecast with the long short-term memory (LSTM) deep learning
35 method. However, the forecast skill for LSTM using only historical observations
36 drops sharply after the first 24 hours. This study implies the potential of improving
37 flood forecast over a cascade reservoir catchment by integrating meteorological
38 forecast, hydrological modeling and machine learning.



39 **Keywords:** Streamflow; Hydrological modeling; LSTM; Reservoir; Ensemble
40 forecast
41



42 **1. Introduction**

43 Flood events are the most destructive ones among the natural disasters, causing
44 huge damages to human society. Reservoirs are massively constructed to regulate
45 river flows, which has significantly reduced flood risks or damages (Ji et al., 2020).
46 However, the number and intensity of precipitation extreme events are increasing in
47 many areas as the global warming continues, thus amplify the potential of flood
48 hazards (Hao et al., 2013; Shao et al., 2016; Wei et al., 2018; Yuan et al., 2018a;
49 Wang et al., 2019). Accurate streamflow forecast is thus needed to provide guidelines
50 for reservoir operations (Robertson et al., 2013), especially when the flood risk is
51 increasing under global warming.

52 A common approach of streamflow forecast is to use hydrological models, where
53 the first attempt could be traced back to 1850s, using simple regression-type
54 approaches to predict discharge from observed precipitation (Mulvaney, 1850). Since
55 then, model concepts have been further augmented by designing new data networks,
56 addressing heterogeneity of hydrological processes, capturing the nonlinear
57 characteristics of hydrologic system and parameterizing models (Hornberger and
58 Boyer, 1995; Kirchner, 2006). With the advancements of computer technology and
59 high-resolution observation, a well-parameterized hydrological model can simulate
60 streamflow with high accuracy (Kollet et al., 2010; Ye et al., 2014; Graaf et al., 2015;
61 Yuan et al., 2018b).



62 Streamflow simulations from hydrological models heavily rely on
63 meteorological forcing inputs, especially precipitation, which can be measured at
64 in-situ gauges or retrieved from satellites and radars. However, for medium-range (2–
65 15 days ahead) streamflow forecasts, precipitation forecast is needed (Hopson et al.,
66 2002). To improve the forecast, ensemble techniques that can give a deterministic
67 estimate as well as its uncertainty became popular. Ensemble weather forecasting can
68 be traced back to 1963 when Leith transferred a deterministic forecast into an
69 ensemble using the Monte-Carlo method to describe the atmospheric uncertainty
70 (Leith, 1963). In the 1990s, ensemble forecasting was developed into an integral part
71 of numerical weather prediction, which showed higher skill than the deterministic
72 forecast even with higher model resolution (Toth et al., 2001). Due to its rapid
73 development, ensemble weather forecasts and climate predictions are applied to
74 hydrological forecasting studies by combining with hydrological models (Jasper et al.,
75 2002; Balint et al., 2006; Jaun et al., 2008; Xu et al., 2015; Yuan et al., 2016; Zhu et
76 al., 2019). Provided with streamflow variability, a reservoir can maintain a reliable
77 utility from natural streamflow better than provided with a deterministic streamflow
78 forecast (Zhao et al., 2011). However, the streamflow prediction skill depends on
79 whether the precipitation forecasts introduced into the hydrological model are skillful
80 (Alfieri et al., 2013). When assessing the skill of this hydrometeorological forecast
81 approach, a benchmark is needed. Using ensembles of historical climatology data
82 (Day, 1985) as meteorological forecast inputs, which is known as ensemble
83 streamflow prediction (ESP), is often selected as the benchmark approach.



84 Evaluations of hydrological forecasts indicated that forecast skill has a close
85 relationship with catchment size, geographical locations and resolutions (Alfieri et al.,
86 2013; Pappenberger et al., 2015), which means there is a necessity to compare with
87 the ESP to show the skill of the hydrometeorological forecast approach.

88 Although physically based hydrological models are widely used, it is still hard
89 to apply a hyper-resolution distributed model for streamflow forecasting due to its
90 demand for observation data, complex model structures and computational resources
91 requirements for calibration and application (Wood et al., 2011; Kratzert et al., 2018;
92 Yaseen et al., 2018). In cascade reservoir systems, there are two sources of streamflow,
93 one is from the rainfall within the interval basin and the other is from the upstream
94 reservoir discharge. While the rainfall-runoff relationship is well studied, it is
95 challenging to reproduce the reservoir operating rules in a physical model (Gao et al.,
96 2010; Zhang et al., 2016; Dang et al., 2020).

97 Machine learning methods can recognize patterns hidden in input data and can
98 simulate or predict streamflow without explicit descriptions of the underlying physical
99 processes (Kisi et al., 2007; Adnan et al., 2019). Neural networks are suitable for
100 streamflow forecasting among machine learning models, some of them can even
101 outperform physically based hydrological models. For example, Humphrey et al.
102 (2016) showed that their combined Bayesian artificial neural network with GR4J
103 model approach outperforms the GR4J model in monthly streamflow forecasting.
104 Kratzert et al. (2019) showed that the long short-term memory (LSTM)-based



105 approach outperforms a well-calibrated Sacramento Soil Moisture Accounting Model
106 (SAC-SMA). Yang et al. (2020) used the geomorphology-based hydrological model
107 (GBHM) combined with traditional ANN model to simulate daily streamflow, which
108 can provide enough physical evidence and can run with less observation data.
109 Although neural network models are criticized with little physical evidence (Abrahart
110 et al., 2012), their potential in hydrological forecasting is yet to be explored.

111 In this study, we combine the machine learning with hydrometeorological
112 approach for hourly streamflow forecast over a data-limited cascade reservoir
113 catchment located in southwestern China. We use the TIGGE-ECMWF
114 meteorological forecasts to drive a newly developed CSSPv2 high-resolution land
115 surface model (Yuan et al., 2018) to provide runoff and streamflow forecasts, and
116 adjust the results via LSTM model to improve streamflow forecast. We strive to (1)
117 calibrate the hydrological model, (2) bias correct the meteorological forecasts, (3)
118 evaluate the streamflow forecast skill and (4) test the physical-statistical combined
119 approach.

120 **2. Study Area, Data, Model and Method**

121 *2.1 Study Area*

122 The Yantan Hydropower Station is in the middle reaches of Hongshui River in
123 Dahua Yao Autonomous County, Guangxi Province. The Yantan Hydropower Station
124 is the fifth level in the 10-level development of Hongshuihe hydropower base in
125 Nanpanjiang River, connected with upstream Longtan Hydropower Station and the



126 downstream Dahua Hydropower Station. The drainage area between the Longtan
127 Hydropower Station and Yantan Hydropower Station is 8,900 km². The annual mean
128 streamflow at Yantan gauge is 55.5 billion m³. The river passes through karst
129 mountain area, with narrow valley, steep slope and scattered cultivated land, and the
130 average slope is 0.036%. Figure 1 shows the locations of 4 hydrological gauges, with
131 detailed information listed in Table 1.

132 *2.2 Data and Method*

133 *2.2.1 Hydrometeorological observations*

134 There are 97 meteorological observation stations within the catchment (Figure
135 1). Here, observed hourly 2m-temperature, 10m-wind speed, relative humidity,
136 accumulated precipitation and surface pressure data were interpolated into a 5km
137 gridded observation dataset via inverse distance weight method. The hourly surface
138 downward solar radiation data from China Meteorological Administration Land Data
139 Assimilation System (CLDAS) was also interpolated into 5km via bilinear
140 interpolation method. The hourly surface downward thermal radiation (long) was
141 estimated by specific humidity, pressure, temperature. This dataset was used to drive
142 the CSSPv2 land surface hydrological model.

143 The monthly runoff for each 5km grid was estimated by disaggregating control
144 streamflow station observations with the ratio of observed grid monthly precipitation
145 and catchment mean precipitation. The gridded runoff was used to calibrate the
146 CSSPv2 model at each grid (Yuan et al., 2016).



147 *2.2.2 Ensemble Meteorological hindcast data and ESP hindcasts*

148 The TIGGE dataset consists of ensemble forecast data from 10 global Numerical
149 Weather Prediction centers started from October 2006, which has been made available
150 for scientific research, via data archive portals at ECMWF and CMA. TIGGE has
151 become a focal point for a range of research projects, including research on ensemble
152 forecasting, predictability, and the development of products to improve the prediction
153 of severe weather (Bougeault et al., 2010). In this paper, TIGGE data from April to
154 September during 2013-2017 from ECMWF were used as meteorological hindcast
155 data. The 3-hourly meteorological hindcasts for 7-day lead time from 51 ensemble
156 members (including control forecast) were interpolated into 5km resolution via
157 bilinear interpolation. The forecast precipitation and temperature were corrected to
158 match the observational means to remove the biases.

159 The ESP was accomplished by applying historical meteorological forcings (Day,
160 1985). In this paper, the meteorological forcings from the same date as the forecast
161 start date to the next 9 days of each year (excluding the target year) were selected as
162 the ESP forcings. Take April 1st, 2013 as example, the 7-day observations started from
163 April 1st to April 10th (i.e., April 1st-April 7th, April 2nd-April 8th, ..., April 10th-April
164 16th) in the year of 2014, 2015, 2016 and 2017 were selected as the forecast ensemble
165 forcings of the issue date (April 1st), with a total of 40 ensemble members.

166 *2.2.3 CSSPv2 streamflow hindcasts*



167 The physical hydrological model used in this paper is the Conjunctive
168 Surface-Subsurface Process model version 2 (CSSPv2; Yuan et al., 2018). The
169 CSSPv2 model is a distributed, grid-based land surface hydrological model, which
170 was developed from the Common Land Model (Dai et al., 2003, 2004), but with better
171 representations in lateral surface and subsurface hydrological processes and their
172 interactions. The routing model used here employs the kinetic wave equation as
173 covariance function, which is solved via a Newton algorithm. A main reason for
174 adopting this covariance function is that it suits the basin with mountainous terrain.
175 The CSSPv2 model was successfully used to perform a high-resolution (3 km) land
176 surface simulation over the Sanjiangyuan region, which is the headwater of major
177 Chinese rivers (Ji and Yuan, 2018). In this paper, we calibrated CSSPv2 model against
178 monthly estimated runoff to simulate the natural hydrological processes by using the
179 SCE-UA approach (Duan et al., 1994). The calibrated parameters include maximum
180 velocity of baseflow, variable infiltration curve parameter, fraction of maximum soil
181 moisture where non-linear baseflow occurs and fraction of maximum velocity of
182 baseflow where non-linear baseflow begins. The hourly observed streamflow at
183 Yantan hydrological gauge was used to calibrate the CSSPv2 routing model manually,
184 including slope, river density, roughness, width and depth. The observed streamflow
185 at Longtan hydrological gauge were added into the corresponding grid to provide
186 upstream streamflow information. The simulation results were evaluated by
187 calculating the Nash-Sutcliffe efficiency (NSE) with corresponding observation data.



188 After calibration, we drove the CSSPv2 model using 5km regridded and
189 bias-corrected TIGGE-ECMWF forecast forcing during 2013-2017 to provide a set of
190 7-day hindcasts (Figure 2). Streamflow hindcasts both from the ESP and the
191 hydrometeorological approach (TIGGE-ECMWF/CSSPv2) were corrected by
192 matching monthly mean streamflow observations to remove the biases, and the
193 hindcast experiments were termed as ESP-Hydro and Meteo-Hydro (Table 2).

194 2.2.4 LSTM streamflow forecast

195 LSTM is a type of recurrent neural network model which learns from sequential
196 data. The input of the LSTM model includes forecast interval streamflow at the
197 specified forecast step obtained from TIGGE-ECMWF/CSSPv2, historical upstream
198 streamflow observation, and historical streamflow observation at Yantan hydrological
199 gauge. The network was trained on sequences of April to September in 2013-2017,
200 with six historical streamflow observations and one forecast interval streamflow to
201 predict the total streamflow at each forecast time step (Figure 2). The LSTM was
202 calibrated through a cross validation method, by leaving the target year out.

203 Before calibration, all input and output variables were normalized as follows:

$$204 \quad \mathbf{q}_0 = \frac{(\mathbf{q} - \mathbf{q}_{\min})}{(\mathbf{q}_{\max} - \mathbf{q}_{\min})}, \quad (7)$$

205 where \mathbf{q} , \mathbf{q}_{\max} and \mathbf{q}_{\min} are the input variable, the maximum and minimum of the
206 sequence of the variable. The hindcast experiment was termed as
207 Meteo-Hydro-LSTM (Table 2). In addition, we also tried an LSTM streamflow



208 forecast approach which only uses 6-hr historical streamflow data as inputs, and the
209 experiment was termed as LSTM (Table 2).

210 2.3 Evaluation Method

211 The root-mean squared error (RMSE) was used to evaluate the deterministic
212 forecast, i.e., the ensemble means of 51 (ECMWF) or 40 (ESP) forecast members. To
213 evaluate probabilistic forecasts, the Continuous Ranked Probability Score (CRPS)
214 was calculated as follows:

$$215 \quad CRPS = \int_{-\infty}^{\infty} [F(y) - F_o(y)]^2, \quad (1)$$

216 where

$$217 \quad F_o(y) = \begin{cases} 0, & y < \textit{observed value} \\ 1, & y \geq \textit{observed value} \end{cases} \quad (2)$$

218 is a cumulative-probability step function that jumps from 0 to 1 at the point where the
219 forecast variable y equals the observation. The CRPS has a negative orientation
220 (smaller values are better), and it rewards concentration of probability around the step
221 function located at the observed value (Wilks, 2005). The skill score for deterministic
222 forecast was calculated as

$$223 \quad SS_{RMSE} = \frac{RMSE - RMSE_{ref}}{0 - RMSE_{ref}} = 1 - \frac{RMSE}{RMSE_{ref}} . \quad (3)$$

224 The skill score for probabilistic forecast (CRPSS) could be calculated similarly based
225 the CRPS.

226 3. Results



227 *3.1 Evaluation of CSSP calibration*

228 The employed CSSPv2 model is a fully distributed hydrological model and the
229 streamflow is calculated through a process of converting gridded rainfall into runoff
230 and a process of runoff routing. Figure 3 shows the runoff calibration results by
231 calculating the NSE of monthly runoff simulations compared with observed gridded
232 monthly runoff. After calibrating the CSSPv2 runoff model, the NSE of all grids are
233 above 0, which indicates that the runoff simulation results in all grids are more
234 reliable than the climatology method. In addition, grids distributed in the downstream
235 region have better NSE than the upstream grids. The NSE values of the grids in the
236 southern part are greater than 0.5, which accounts for two thirds of the interval basin
237 area.

238 Figures 4 and 5 show the results after the calibration of the routing model, where
239 time series of CSSPv2-simulated streamflow are compared against observed
240 streamflow at Yantan hydrological gauge. Figure 4 shows the daily and monthly
241 streamflow simulation results. The monthly result (Fig. 4f) shows that the simulated
242 streamflow closely follows the observed streamflow, and the NSE is 0.96. The daily
243 streamflow simulations during flood seasons (Figs. 4a-4e) also show a good
244 performance, and the NSE is 0.92. During June and July in years of 2014, 2015 and
245 2017, the CSSPv2 model underestimated the daily streamflow with a maximum of
246 $1104 \text{ m}^3/\text{s}$ and an average of $334 \text{ m}^3/\text{s}$ (Figs. 4b, 4c, 4e). In years of 2013 and 2016,
247 the difference between observed and simulated streamflow is relatively small, and the
248 average difference is $96 \text{ m}^3/\text{s}$ (Figs. 4a, 4d).



249 Figure 5 shows the hourly streamflow simulation results for a few flood events.
250 Figure 5a shows that the CSSPv2 model can accurately simulate the streamflow
251 response to a rainfall event after a dry period. Figures 5b-5d show that for
252 instantaneous heavy rainfall events, the CSSPv2 model over-predicted the water loss
253 during recession period. Figures 5e-5f show that for continuous rainfall events, the
254 simulated streamflow has a larger fluctuation than observation. The simulated
255 streamflow is also smoother than observation. Nevertheless, the NSE for the hourly
256 streamflow simulation is 0.61, which suggests that CSSPv2 has an acceptable
257 performance at hourly time scale.

258 *3.2 Bias correction of TIGGE-ECMWF meteorological forecasts*

259 The resolution of TIGGE-ECMWF grid data is 0.25° , so the data was
260 interpolated to 5km grid to drive the CSSPv2 model. Figure 6 shows the correlation
261 coefficient and RMSE of TIGGE-ECMWF precipitation and temperature forecasts as
262 compared against observations, either before or after bias correction. The 51-ensemble
263 mean precipitation and temperature (the red dashed lines) shows better performance
264 than the best ensemble members (the green dashed lines), with an average RMSE
265 reduction of 3.66 mm/day and average correlation increase of 0.04 for precipitation,
266 and average RMSE reduction of 0.1K and average correlation increase of 0.03 for
267 temperature. After bias correction, the 51-ensemble means still perform better than
268 best ensemble members. Compared with ensemble mean results before bias correction,
269 the RMSE reduced by 0.23 mm/day for the bias-corrected precipitation, and reduced
270 by 1K for the bias-corrected surface air temperature. For the bias-corrected ensemble



271 mean results, the average RMSE and correlation are 14.6 mm/day and 0.44 for
272 precipitation, and 1.25 K and 0.87 for surface air temperature.

273 *3.3 Comparison between ESP-Hydro and Meteo-Hydro streamflow forecast*

274 Figure 7 presents the variations of RMSE and CRPS for ESP-Hydro and
275 Meteo-Hydro hourly streamflow forecast at Yantan hydrological gauge. For
276 probabilistic forecast, Figure 7a shows that the CRPS for Meteo-Hydro streamflow
277 forecast ranges from 160 to 230 while the CRPS for ESP-Hydro streamflow forecast
278 ranges from 183 to 250. The Meteo-Hydro approach performs better than ESP-Hydro
279 with lower CRPS at all lead times, with an average of 10% improvement in CRPSS
280 (Figure 7c). For deterministic forecast, Figure 7b shows that the RMSE for
281 Meteo-Hydro streamflow forecast ranges from 250 to 350 m³/s, while the RMSE for
282 ESP-Hydro streamflow forecast ranges from 250 to 390 m³/s. The Meteo-Hydro
283 approach also performs better than ESP-Hydro with lower RMSE at all lead times
284 especially after 3 days, with the average reduction of RMSE reaching 6% (Figure 7d).

285 Figure 7 also shows that both forecast skills have a similar diurnal cycle, where
286 RMSE and CRPS reach their peaks around 00UTC and drop to their lows at 06UTC.
287 Figure 8 shows the diurnal cycle of model employed variables, which are observed
288 catchment mean rainfall, observed streamflow at Yantan and Longtan hydrological
289 gauges, to explain the diurnal cycle of ESP-Hydro and Meteo-Hydro forecasting skills.
290 These three input variables show different diurnal patterns. The observed rainfall
291 starts to rise at 00UTC and reaches its maximum at 06UTC. The observed streamflow
292 at Yantan hydrological gauge drops to its minimum at 12UTC and rises to its



293 maximum at 00UTC. The streamflow from upstream Longtan hydrological gauge
294 starts to drop at 00UTC and reaches its minimum at 06UTC. After comparing these
295 diurnal cycles with the cycle of forecast skill, it is found that the forecast skill
296 decreases when the upstream Longtan outflow starts to decrease, and the precipitation
297 starts to increase. When the upstream Longtan outflow increases and the precipitation
298 starts to decrease (after 06UTC), the forecast skill rises. Such information indicates
299 that the hydrological model performs worse in the case of heavier rainfall event, and
300 the decrease of upstream outflow may amplify such degradation when the portion of
301 interval rainfall-runoff increased.

302 *3.4 Meteo-Hydro-LSTM streamflow forecast*

303 Machine learning methods can recognize patterns hidden in input data and can
304 simulate or predict streamflow without explicit descriptions of the underlying physical
305 processes. Figure 9 shows the RMSE of Meteo-Hydro-LSTM streamflow forecast
306 using the ensemble mean hydrological forecast as described in the section above, and
307 the past 6-hour observed streamflow of Yantan hydrological gauge as input.
308 Compared with Meteo-Hydro and ESP-Hydro approach, applying LSTM model can
309 further decrease the RMSE within the first 72 hours. The RMSE of
310 Meteo-Hydro-LSTM approach ranges from 205 to 363 m³/s during these three days,
311 suggesting an average of 6% improvement against Meteo-Hydro approach.

312 Figure 9 also shows the RMSE of LSTM streamflow forecast only using the past
313 6-hour observed streamflow of Yantan hydrological gauge as input. Without using the



314 physical model forecast, RMSE is improved only when the lead time is less than 1 day.
315 And the performance of LSTM is far worse than Meteo-Hydro streamflow forecast
316 when lead time is more than 2 days.

317 Figure 10 shows several examples of streamflow forecasts by
318 Meteo-Hydro-LSTM approach and Meteo-Hydro approaches to show the forecast
319 improvements in details. The Meteo-Hydro-LSTM approach reduced the flood peak
320 value and the water loss during flood recession period compared with Meteo-Hydro
321 streamflow forecast approach, which improves the streamflow prediction for most
322 cases (Figs. 10b-10f). However, when the upstream reservoir's flood operation is
323 triggered by continuous heavy rain, the Meteo-Hydro may underpredict the
324 streamflow. With the LSTM model further decreases the streamflow, the
325 Meteo-Hydro-LSTM method can end up with worsening the streamflow forecast,
326 which means the machine learning method may improve forecasts when trained in
327 different flood operating situations (Figure 10a).

328 **4. Conclusions**

329 In this study, we developed and evaluated a streamflow forecasting framework
330 by coupling meteorological forecasts with a land surface hydrological model (CSSPv2)
331 and a machine learning method (LSTM) over a cascade reservoir catchment using
332 hindcast data from 2013 to 2017. The monthly observed runoff was used to calibrate
333 the runoff generation module of the CSSPv2 model grid by grid, and the hourly
334 observed streamflow at Yantan hydrological gauge was used to calibrate the routing



335 module of the CSSPv2 model. Then, the bias-corrected TIGGE-ECMWF ensemble
336 forecasts were used to drive the CSSPv2 for streamflow forecasts, and the LSTM
337 model was used to correct the streamflow forecasts, resulted in an integrated
338 meteorological-hydrological-machine learning forecast framework.

339 With automatic offline calibration of the CSSPv2 model, and the NSE values are
340 0.96, 0.92 and 0.61 for streamflow simulations at the Yantan gauge at monthly, daily
341 and hourly time scales, respectively. The bias-corrected ensemble mean
342 TIGGE-ECMWF forcings which perform the best among all ensemble members,
343 show average RMSE and correlation of 14.6 mm/day and a 0.44 for precipitation
344 forecasts, and 1.3 K and 0.87 for surface air temperature forecasts. By comparing with
345 the hourly observed streamflow, the integrated hydrometeorological forecast approach
346 (Meteo-Hydro) increases the probabilistic and deterministic forecast skill against the
347 initial condition-based approach (ESP-Hydro) by 10% (CRPSS) and 6% (RMSE skill
348 score), respectively .

349 Adding LSTM model to the hydrometeorological forecast (Meteo-Hydro-LSTM)
350 can further reduce the forecast error. Within the first 72 hours, LSTM can improve the
351 forecast skill with a maximum of 25% and an average of 6%. However, if we do not
352 use the streamflow predicted by Meteo-Hydro, the error from the LSTM increases
353 rapidly after 24 hours, and the historical data-based LSTM method performs worse
354 than the Meteo-Hydro method.

355



356 **Acknowledgement.** This work was supported by National Key R&D Program of
357 China (2018YFA0606002), and National Natural Science Foundation of China
358 (41875105).

359

360 **Data availability.** The TIGGE-ECMWF hindcast data can be downloaded from
361 <https://apps.ecmwf.int/datasets/data/tigge/levtype=sfc/type=pf/> (Parsons et al., 2017),
362 the in-situ observations and simulation data are available upon request.

363



364 **References**

- 365 Abrahart, R. J., Anctil, F., Coulibaly, P., Dawson, C. W., Mount, N. J., See, L. M., et
366 al.: Two decades of anarchy? emerging themes and outstanding challenges for
367 neural network river forecasting. *Prog. Phys. Geogr.* 36(4), 480-513.
368 <https://doi.org/10.1177/0309133312444943>, 2012.
- 369 Adnan, R.M., et al.: Daily streamflow prediction using optimally pruned extreme
370 learning machine. *J. Hydrol.* 577. <https://doi.org/10.1016/j.jhydrol.2019.123981>,
371 2019.
- 372 Alfieri, L., Burek, P., Dutra, E., Krzeminski, B., & Pappenberger, F.: GloFAS-global
373 ensemble streamflow forecasting and flood early warning. *Hydrol. Earth Syst.*
374 *Sci.* 17 (3), 1161–1175. <https://doi.org/10.5194/hess17-1161-2013>, 2013.
- 375 Balint, G., Csik, A., Bartha, P., Gauzer, B., Bonta, I.: Application of meteorological
376 ensembles for Danube flood forecasting and warning. In: Marsalek, J., Stancalie,
377 G., Balint, G. (Eds.), *Transboundary Floods: Reducing Risks through Flood*
378 *Management*. Springer, NATO Science Series, Dordrecht, The Netherlands, pp.
379 57–68. https://doi.org/10.1007/1-4020-4902-1_6, 2006.
- 380 Bougeault, P., et al.: The THORPEX interactive grand global ensemble, *Bull. Am.*
381 *Meteorol. Soc.*, 91, 1059–1072. <http://dx.doi.org/10.1175/2010BAMS2853.1>,
382 2010.
- 383 Dai, Y., Dickinson, R. E., Wang, Y. P.: A two-big-leaf model for canopy temperature,
384 photosynthesis, and stomatal conductance. *J. Clim.* 17(12),2281–2299.
385 [https://doi.org/10.1175/1520-0442\(2004\)017<2281:ATMFCT>2.0.CO;2](https://doi.org/10.1175/1520-0442(2004)017<2281:ATMFCT>2.0.CO;2), 2004.



- 386 Dai, Y., Zeng, X., Dickinson, R. E., Baker, I., Bonan, G. B., Bosilovich, M. G., et al.:
- 387 The Common Land Model. *Bull. Am. Meteorol. Soc.* 84(8), 1013–1024.
- 388 <https://doi.org/10.1175/BAMS-84-8-1013>, 2003.
- 389 Dang, T. D., Chowdhury, A. K., Galelli, S.: On the representation of water reservoir
- 390 storage and operations in large-scale hydrological models: implications on
- 391 model parameterization and climate change impact assessments. *Hydrol. Earth*
- 392 *Syst. Sci.*, 24, 397–416. <https://doi.org/10.5194/hess-24-397-2020>, 2020.
- 393 Day, G.N.: Extended Streamflow Forecasting Using NWSRFS. *J. Water Resour. Plan*
- 394 *Manag.* 111 (2): 157-170, 1985.
- 395 Duan, Q., Sorooshian, S., Gupta, V. K.: Optimal use of SCEUA global optimization
- 396 method for calibrating watershed models, *J. Hydrol.*, 158, 265–284,
- 397 [https://doi.org/10.1016/0022-1694\(94\)90057-4](https://doi.org/10.1016/0022-1694(94)90057-4), 1994.
- 398 Gao, X., Zeng, Y., Wang, J., Liu, H.: Immediate impacts of the second impoundment
- 399 on fish communities in the Three Gorges Reservoir, *Environ. Biol. Fish.*, 87,
- 400 163–173. <https://doi.org/10.1007/s10641-009-9577-1>, 2010.
- 401 Graaf, I. D., Sutanudjaja, E. H., Beek, L. V., et al.: A high-resolution global-scale
- 402 groundwater model. *Hydrol. Earth Syst. Sci.* 19(2):823-837.
- 403 <https://doi.org/10.5194/hess-19-823-2015>, 2015.
- 404 Hao, Z., Aghakouchak, A., Phillips, T. J.: Changes in concurrent monthly precipitation
- 405 and temperature extremes. *Environ. Res. Lett.* 8(3), 1402-1416.
- 406 <https://doi.org/10.1088/1748-9326/8/3/034014>, 2013.
- 407 Hopson, T., Webster, P.: A 1–10 day ensemble forecasting scheme for the major river



- 408 basins of Bangladesh: forecasting severe floods of 2003–2007. *J. Hydrometeorol.*
409 11(3), 618–641. <https://doi.org/10.1175/2009JHM1006.1>, 2010.
- 410 Hornberger, G. M., E. W. Boyer.: Recent advances in watershed modeling, U.S. Natl.
411 Rep. Int. Union Geod. Geophys. 1991 – 1994, *Rev. Geophys.*, 33, 949 – 957.
412 <https://doi.org/10.1029/95RG00288>, 1995.
- 413 Humphrey, G.B., Gibbs, M.S., Dandy, G.C., Maier, H.R.: A hybrid approach to
414 monthly streamflow forecasting: Integrating hydrological model outputs into a
415 Bayesian artificial neural network. *J. Hydrol.* 540, 623–640.
416 <https://doi.org/10.1016/j.jhydrol.2016.06.026>, 2016.
- 417 Jasper, K., Gurtz, J., Lang, H.: Advanced flood forecasting in Alpine watersheds by
418 coupling meteorological observations and forecasts with a distributed
419 hydrological model. *J. Hydrol.* 267 (1–2), 40–52.
420 [https://doi.org/10.1016/S0022-1694\(02\)00138-5](https://doi.org/10.1016/S0022-1694(02)00138-5), 2002.
- 421 Jaun, S., Ahrens, B., Walser, A., Ewen, T., Schär, C.: A probabilistic view on
422 the August 2005 floods in the upper Rhine catchment. *Nat. Hazard Earth Sys.* 8,
423 281–291. <https://doi.org/10.5194/nhess-8-281-2008>, 2008.
- 424 Ji, P., X. Yuan., Y. Jiao., C. Wang., S. Han., C. Shi.: Anthropogenic contributions to
425 the 2018 extreme flooding over the upper Yellow River basin in China. *Bull. Am.*
426 *Meteorol. Soc.* 101(1), S89–S94, <https://doi.org/10.1175/BAMS-D-19-0105.1>,
427 2020.
- 428 Kirchner, J. W.: Getting the right answers for the right reasons: Linking measurements,
429 analyses, and models to advance the science of hydrology, *Water Resour. Res.*



- 430 42, 1–5. <https://doi.org/10.1029/2005WR004362>, 2006.
- 431 Kisi, O.: Streamflow forecasting using different artificial neural network algorithms. J.
432 Hydrol. Eng. 12 (5), 532–539.
433 [https://doi.org/10.1061/\(ASCE\)1084-0699\(2007\)12:5\(532\)](https://doi.org/10.1061/(ASCE)1084-0699(2007)12:5(532)), 2007.
- 434 Kollet, S. J., Maxwell, R. M., Woodward, C. S., Smith, S., Vanderborght, J., &
435 Vereecken, H., et al.: Proof of concept of regional scale hydrologic simulations
436 at hydrologic resolution utilizing massively parallel computer resources. Water
437 Resour. Res. 46(4). <https://doi.org/10.1029/2009WR008730>, 2010.
- 438 Kratzert, F., Klotz, D., Brenner, C., Schulz, K., Herrnegger, M.: Rainfall–runoff
439 modelling using long short-term memory (LSTM) networks. Hydrol. Earth Syst.
440 Sci. 22 (11), 6005–6022. <https://doi.org/10.5194/hess-22-6005-2018>, 2018.
- 441 Kratzert, F., Klotz, D., Herrnegger, M., Sampson, A. K., Hochreiter, S., Nearing, G. S.:
442 Towards Improved Predictions in Ungauged Basins: Exploiting the Power of
443 Machine Learning. Water Resour. Res. 55.
444 <https://doi.org/10.1029/2019wr026065>, 2019.
- 445 Leith, C. E.: Theoretical skill of monte carlo forecasts. Mon. Weather Rev. 102(6),
446 409-418. [https://doi.org/10.1175/1520-0493\(1974\)102<0409:CO:2](https://doi.org/10.1175/1520-0493(1974)102<0409:CO:2), 1974.
- 447 Mulvaney, T. J.: On the use of self-registering rain and flood gauges in making
448 observations of the relations of rainfall and of flood discharges in a given
449 catchment, in: Proceedings Institution of Civil Engineers, Dublin, Vol. 4, 18–31,
450 1850.
- 451 Pappenberger, F., Ramos, M. H., Cloke, H. L., Wetterhall, F., Alfieri, L., Bogner, K.,



- 452 et al.: How do I know if my forecasts are better? Using benchmarks in
453 hydrological ensemble prediction. *J. Hydrol.* 522, 697–713.
454 <https://doi.org/10.1016/j.jhydrol.2015.01.024>, 2015.
- 455 Parsons, D. B., Beland, M., Burridge, D., Bougeault, P., Brunet, G., Caughey, J., et al.:
456 Thorpex research and the science of prediction. *Bull. Am. Meteorol. Soc.*, 98,
457 807-830, <https://doi.org/10.1175/BAMS-D-14-00025.1>, 2017.
- 458 Robertson, D. E., Wang, Q. J.: Seasonal Forecasts of Unregulated Inflows into the
459 Murray River, Australia. *Water Resour. Manag.* 27(8):2747–2769.
460 <https://doi.org/10.1007/s11269-013-0313-4>, 2013.
- 461 Shao, J., Wang, J., Lv, S., Bing, J.: Spatial and temporal variability of seasonal
462 precipitation in Poyang Lake basin and possible links with climate indices.
463 *Hydrol. Res.* 47(S1):51–68. <https://doi.org/10.2166/nh.2016.249>, 2016.
- 464 Toth, Z., Zhu, Y., Marchok, T.: The use of ensembles to identify forecasts with small
465 and large uncertainty. *Weather Forecast* 16(4), 463-463.
466 [https://doi.org/10.1175/1520-0434\(2001\)0162.0.CO;2](https://doi.org/10.1175/1520-0434(2001)0162.0.CO;2), 2001.
- 467 Wang, R., Zhang, J., Guo, E., Zhao, C., Cao, T.: Spatial and temporal variations of
468 precipitation concentration and their relationships with large-scale atmospheric
469 circulations across Northeast China. *Atmos. Res.* 222:62–73.
470 <https://doi.org/10.1016/j.atmosres.2019.02.008>, 2019.
- 471 Wilks, D. S.: *Statistical Methods in the Atmospheric Sciences*, Volume 91, Second
472 Edition (International Geophysics), 2005.
- 473 Wood, E. F., et al.: Hyperresolution global land surface modeling: Meeting a grand



- 474 challenge for monitoring Earth's terrestrial water. *Water Resour. Res.*, 47,
475 W05301, <https://doi.org/10.1029/2010WR010090>, 2011.
- 476 Xu, Y.P., Gao, X., Zhang, Y., Kang, L.: Coupling a regional climate model and
477 distributed hydrological model to assess future water resources in Jinhua River
478 Basin, East China. *ASCE. J. Hydrol. Eng.* 20, 2015,
479 [https://doi.org/10.1061/\(ASCE\)HE.1943-5584.0001007](https://doi.org/10.1061/(ASCE)HE.1943-5584.0001007), 2015.
- 480 Yang, S., Yang, D., Chen, J., Santisirisomboon, J., Zhao, B.: A physical process and
481 machine learning combined hydrological model for daily streamflow
482 simulations of large watersheds with limited observation data. *J. Hydrol.* 590,
483 125206. <https://doi.org/10.1016/j.jhydrol.2020.125206>, 2020.
- 484 Yaseen, Z.M., Sulaiman, S.O., Deo, R.C., Chau, K.-W.: An enhanced extreme learning
485 machine model for river flow forecasting: State-of-the-art, practical applications
486 in water resource engineering area and future research direction. *J. Hydrol.* 569,
487 387–408. <https://doi.org/10.1016/j.jhydrol.2018.11.069>, 2018.
- 488 Ye, A., Duan, Q., Yuan, X., Wood, E. F., Schaake, J.: Hydrologic post-processing of
489 MOPEX streamflow simulations. *J. Hydrol.* 508, 147-156,
490 doi:10.1016/j.jhydrol.2013.10.055, 2014
- 491 Yuan, X., Ma, F., Wang, L., Zheng, Z., Ma, Z., Ye A., Peng, S.: An experimental
492 seasonal hydrological forecasting system over the Yellow River basin-Part 1:
493 Understanding the role of initial hydrological conditions. *Hydrol. Earth Syst. Sci.*
494 20, 2437–2451, <https://doi.org/10.5194/hess-20-2437-2016>, 2016.
- 495 Yuan, X., S. Wang, and Z.-Z. Hu, 2018a: Do climate change and El Niño increase



496 likelihood of Yangtze River extreme rainfall? Bull. Am. Meteorol. Soc. 99,
497 S113-S117, <https://doi.org/10.1175/BAMS-D-17-0089.1>, 2018a.

498 Yuan, X., Ji, P., Wang, L., Liang, X. Z., Yang, K., Ye, A., et al.: High - resolution land
499 surface modeling of hydrological changes over the sanjiangyuan region in the
500 eastern tibetan plateau: 1. model development and evaluation. J. Adv. Model
501 Earth Syst. <https://doi.org/10.1029/2018MS001412>, 2018b.

502 Zhang, Y., Erkyihum, S. T., Block, P.: Filling the GERD: evaluating hydroclimatic
503 variability and impoundment strategies for Blue Nile riparian countries, Water
504 Int., 41, 593–610. <https://doi.org/10.1080/02508060.2016.1178467>, 2016.

505 Zhao, T.T.G., Cai, X.M., Yang, D.W.: Effect of streamflow forecast uncertainty on
506 real-time reservoir operation. Adv. Water Resour. 34 (4), 495–504,
507 <https://doi.org/10.1016/j.advwatres.2011.01.004>, 2011.

508 Zhu, E., X. Yuan., A. Wood.: Benchmark Decadal Forecast Skill for Terrestrial Water
509 Storage Estimated by an Elasticity Framework. Nat. Commun. 10, 1237,
510 <https://doi.org/10.1038/s41467-019-09245-3>, 2019.

511



512 **Table 1.** Information of hydrological gauges.

Gauge	Longitude ($^{\circ}$ E)	Latitude ($^{\circ}$ N)	Drainage area (km^2)
Longtan	107.09	25.00	-
Yantan	107.50	24.11	5950 (orange area in Fig. 1)
Luofu	107.36	24.90	800 (green area in Fig. 1)
Jiazhuan	107.12	24.21	2150 (purple area in Fig. 1)

513



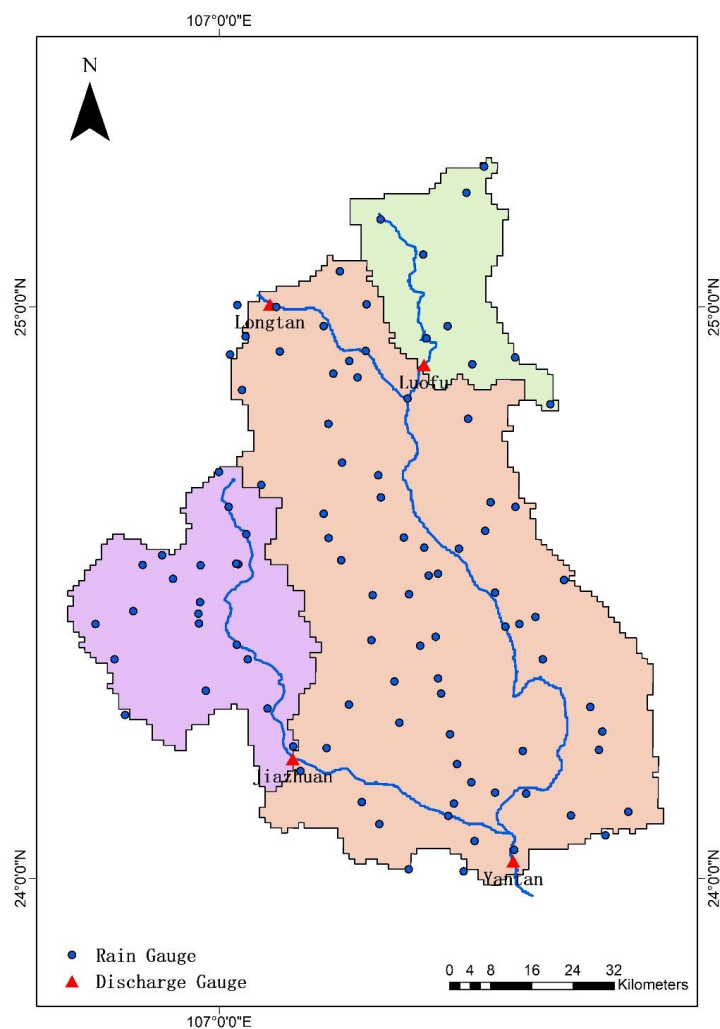
514 **Table 2.** Experimental design in this study.

Experiments	Description
ESP-Hydro	Using CSSPv2 land surface hydrological model driven by randomly-sampled historical meteorological forcings
Meteo-Hydro	Using CSSPv2 model driven by bias-corrected TIGGE-ECMWF hindcast meteorological forcings
Meteo-Hydro-LSTM	Using LSTM model to correct streamflow from Meteo-Hydro hindcast
LSTM	Using LSTM model to forecast streamflow based on observation only

515



516

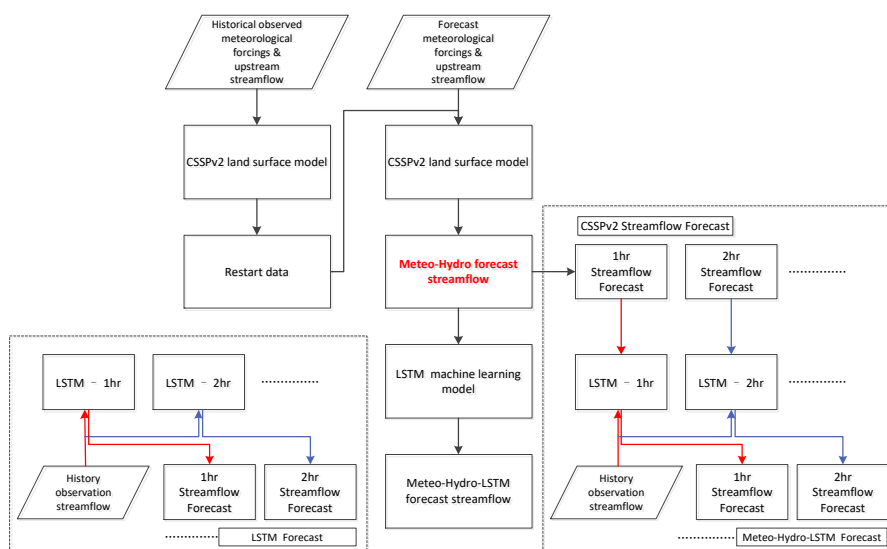


517

518 **Figure 1.** Locations of discharge gauges and rain gauges over the Yantan basin.



519



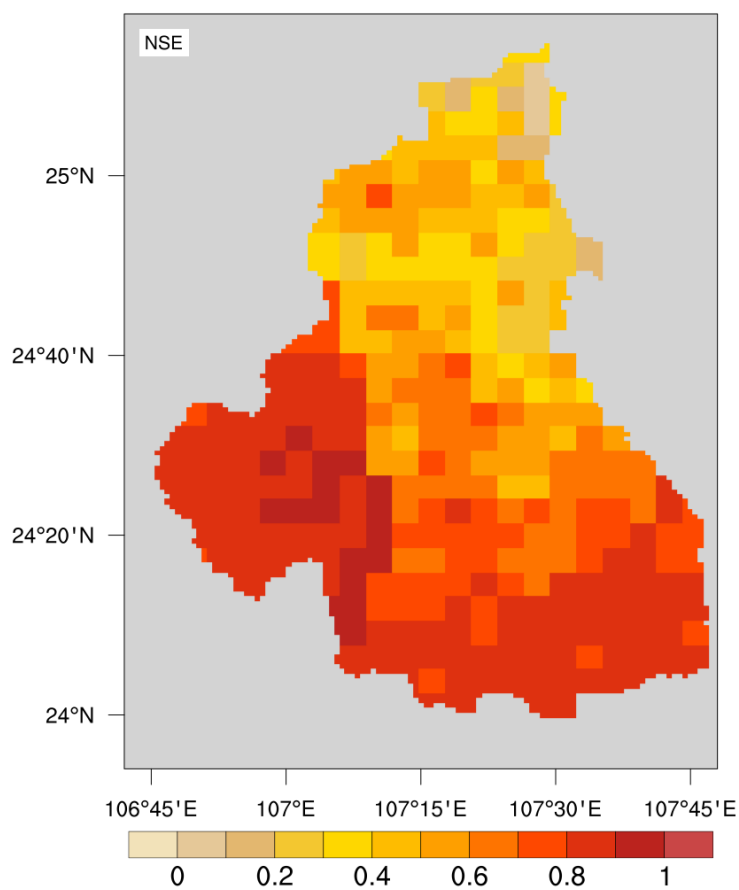
520

521 **Figure 2.** A diagram for the integrated hydrometeorological and machine learning

522 streamflow prediction.



523



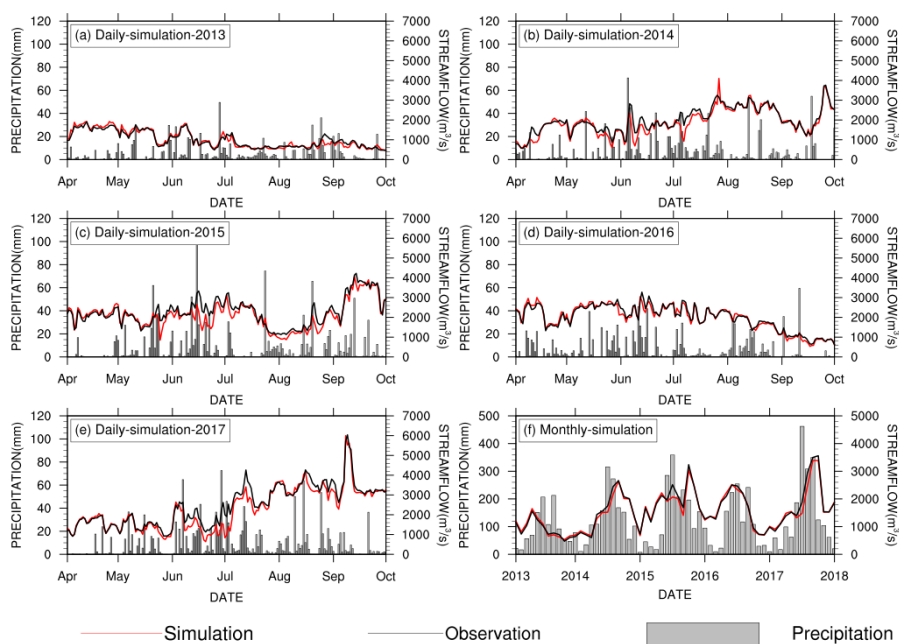
524

525 **Figure 3.** Nash-Sutcliffe efficiency coefficients for the calibrated grid runoff simulation

526 from CSSPv2.



527

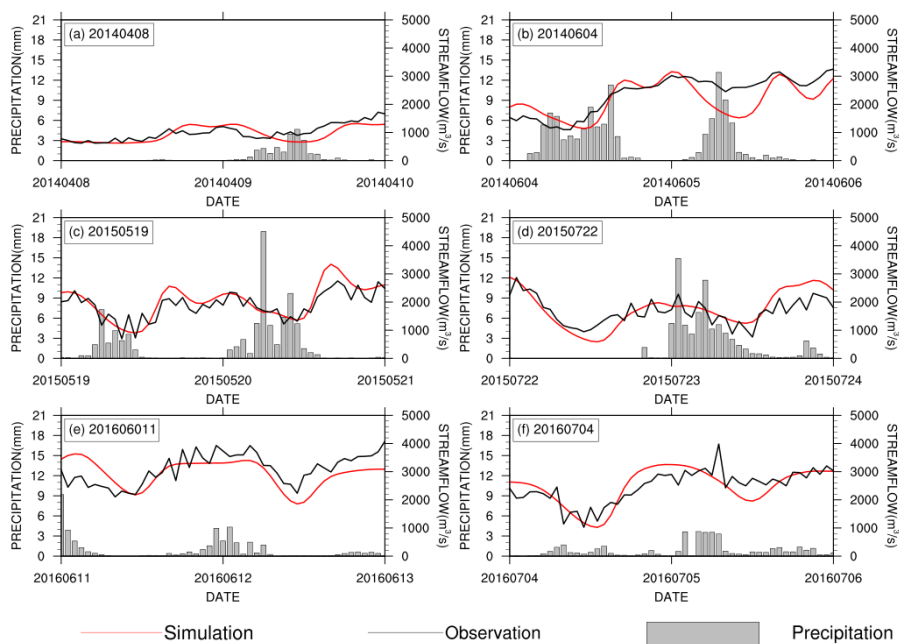


528

529 **Figure 4.** Evaluation of streamflow simulations at Yantan gauge. The black and red
530 lines are observed and simulated streamflow. (a)-(e) are for daily streamflow, and (f)
531 is for monthly streamflow. The gray bars represent daily (or monthly) precipitation.



532



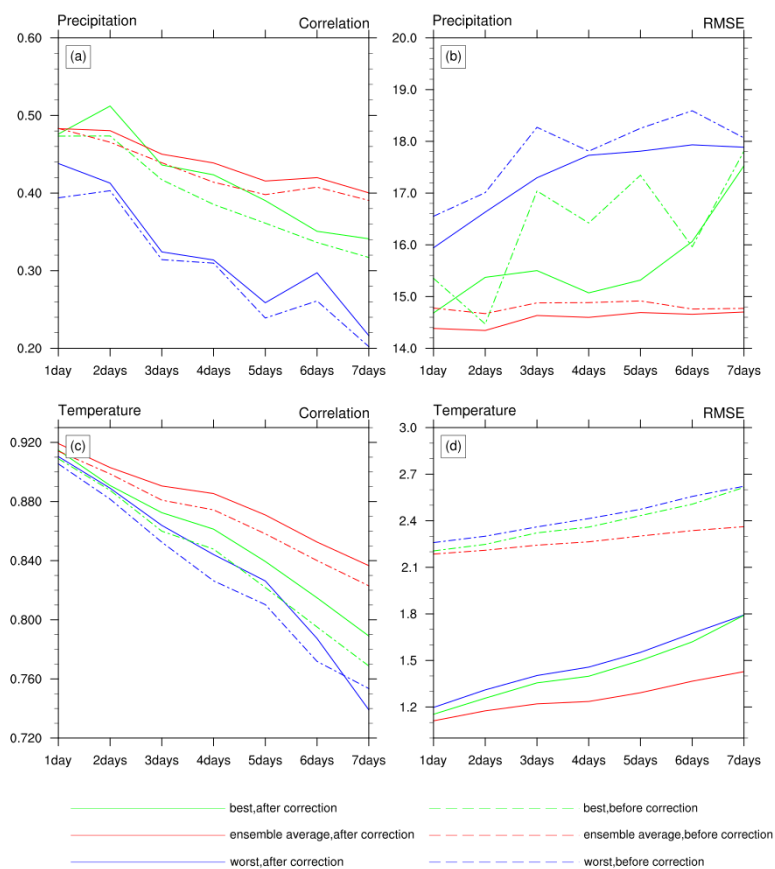
533

534 **Figure 5.** The same as Figure 4, but for the evaluation of hourly streamflow

535 simulations at Yantan gauge.



536

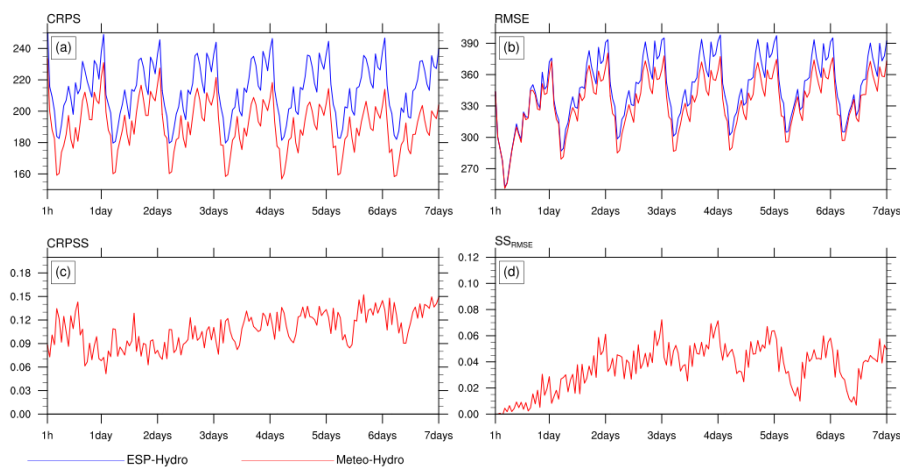


537

538 **Figure 6.** Evaluation of precipitation and temperature hindcasts from
539 TIGGE-ECMWF. The red and blue lines represent the best and worst results among 51
540 TIGGE-ECMWF ensemble members respectively, and the green lines represent the
541 results for the ensemble means of 51 members. Solid and dashed lines represent the
542 results after and before bias corrections, respectively.



543

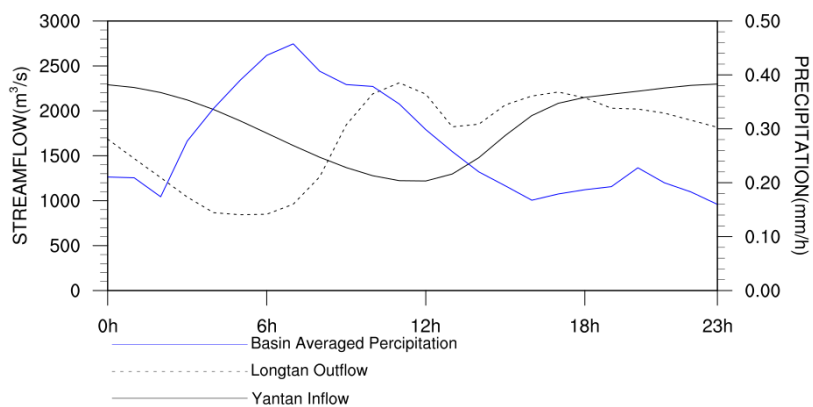


544

545 **Figure 7.** (a) Continuous Ranked Probability Score (CRPS) and (b) Root Mean
546 Squared Error (RMSE) for daily streamflow ensemble forecasts at Yantan gauge. (c)
547 and (d) are the skill score in terms of CRPS and RMSE for Meteo+Hydro, where
548 ESP+Hydro is used as reference forecast.



549

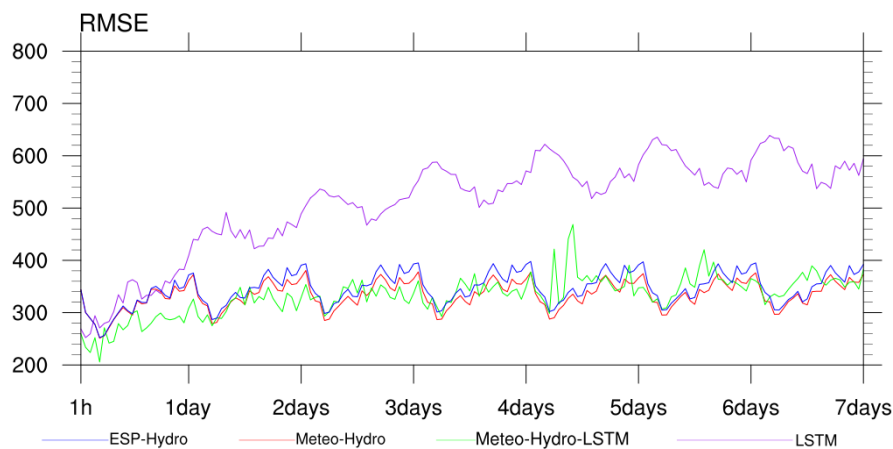


550

551 **Figure 8.** Diurnal cycle of Longtan outflow (m^3/s ; dashed black line), Yantan inflow
552 (m^3/s ; solid black line) and basin-averaged precipitation (mm/h ; blue line).

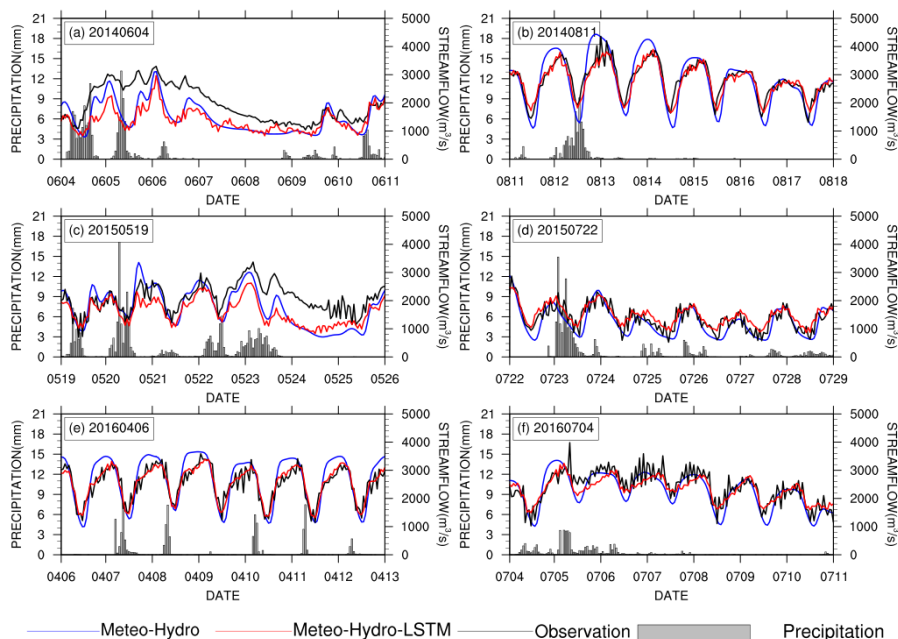


553



554

555 **Figure 9.** RMSE (m^3/s) for hourly streamflow hindcasts from four forecast
556 approaches. The green line represents the Meteo+Hydro+LSTM forecast, the red line
557 represents the Meteo+Hydro forecast, the blue line represent the ESP+Hydro forecast,
558 and the purple line represents the LSTM forecast based on historical streamflow
559 observation alone.



560

561 **Figure 10.** Evaluation of the forecast approaches for a few flooding events. The black
562 lines are observed streamflow from Yantan hydrological gauge, the blue lines are the
563 Meteo+Hydro ensemble mean streamflow forecast, and the red lines are the
564 Meteo+Hydro+LSTM forecast streamflow by using Meteo+Hydro ensemble mean
565 forecast with LSTM. The gray bars represent hourly precipitation averaged over the
566 basin.